Letter

Nuclear-matter saturation and symmetry energy within Δ-full chiral effective field theory

W. G. Jiang,[1,2] C. Forssén,[1] T. Djärv,[1,3] and G. Hagen[3,4]

[1]*Department of Physics, Chalmers University of Technology, SE-412 96 Göteborg, Sweden*

[2]*Institut für Kernphysik and PRISMA Cluster of Excellence, Johannes Gutenberg Universität, 55128 Mainz, Germany*

[3]*Physics Division, Oak Ridge National Laboratory, Oak Ridge, Tennessee 37831, USA*

[4]*Department of Physics and Astronomy, University of Tennessee, Knoxville, Tennessee 37996, USA*

(Received 16 January 2023; revised 19 March 2024; accepted 3 June 2024; published 12 June 2024)

Nuclear saturation and the symmetry energy are key properties of low-energy nuclear physics that depend on fine details of the nuclear interaction. The equation of state around saturation is also an important anchor for extrapolations to higher densities and studies of neutron stars. Here we develop a unified statistical framework that uses realistic nuclear forces to link the theoretical modeling of finite nuclei and infinite nuclear matter. We construct fast and accurate emulators for nuclear-matter observables and employ an iterative history-matching approach to explore and reduce the enormous parameter domain of Δ-full chiral interactions. We perform rigorous uncertainty quantification and find that model calibration including ^{16}O observables gives saturation predictions that are more precise than those that only use few-body data.

DOI: 10.1103/PhysRevC.109.L061302

Introduction. A key question in low-energy nuclear physics is whether it is possible to successfully describe all systems from finite nuclei to infinite nuclear matter using nucleons as effective degrees of freedom. Realistic interaction models based on chiral effective field theory (χEFT) used in combination with *ab initio* methods, that solve the many-body problem with controlled approximations, have the potential to deliver on that research program [1–9]. However, using a complicated interaction model and calibration data with limited independence implies a risk for overfitting unless relevant theoretical uncertainties are accounted for. Furthermore, the extrapolation from well-studied few-nucleon systems to heavier nuclei and infinite nuclear matter will lead to increasing variances in model predictions. Therefore it becomes important to study the precision of these predictions and to explore the sensitivity to different choices of calibration data. The emergence of nuclear saturation—represented by a minimum in the equation of state (EOS) for infinite symmetric nuclear matter (SNM)—is particularly important since it affects bulk properties (such as binding energies and radii) of finite atomic nuclei. Furthermore, the density dependence of the EOS for pure neutron matter (PNM) is central for the physics of neutron stars [10–12].

In the last decade significant progress has been made towards quantifying EFT uncertainties of *ab initio* nuclear matter predictions and identifying possible correlations with observables in finite nuclei [2,7,13–20]. Very recently, some of the authors of this work identified correlations between the symmetry energy and its slope with the neutron skin and dipole polarizability of the heavy nucleus ^{208}Pb starting from chiral interactions at next-to-next-to-leading order (NNLO) with explicit delta isobars (Δ) [7]. This finding was made possible by employing novel statistical tools such as Bayesian inference [21] and history matching [7,22–24] together with accurate emulators of *ab initio* computations of light nuclei [25–28].

In this Letter we develop fast and accurate emulators of coupled-cluster computations of PNM and SNM [29,30] starting from Δ-full χEFT interaction models at NNLO [5,31–36]. Our construction of emulators is based on the subspace-projected coupled cluster (SPCC) method [25], which we here extend with small batch voting [37]—a new on-the-fly validation approach that addresses the possible appearance of spurious states when diagonalizing a Hamiltonian in a subspace of biorthogonal coupled-cluster solutions [38]. Using these emulators we can reproduce full-space coupled-cluster computations of infinite nuclear matter with high precision at a tiny fraction of the computational cost.

After validating our approach, we use history matching to identify a region of the 17-dimensional parameter space of the low-energy constants (LECs) at NNLO that give acceptable results when confronted with few-body data. This iterative parameter search is enabled by employing emulators of few-body systems up to ^{4}He and allows us to collect 1.7×10^6 nonimplausible interaction samples. Finally, we calibrate our *ab initio* model with two alternative LEC posterior probability density functions (PDFs) and use the principle of importance resampling [39,40] to quantify the sensitivity of nuclear matter predictions to calibration data. Here we focus on the results of this analysis, and the emergence of nuclear saturation, while details of the small-batch voting scheme and the history match are presented in a companion paper [37].

Method. The chiral Hamiltonian of ΔNNLO is parametrized with 17 LECs [5], and following Refs. [25–27] it can be written as

$$H(\alpha) = h_0 + \sum_{i=1}^{N_{\rm LECs}=17} \alpha_i h_i. \quad (1)$$

Here, $h_0 = t_{\rm kin} + v_0$, where $t_{\rm kin}$ is the kinetic energy and v_0 represents the constant potential term without LEC dependence. Note that $\vec{\alpha}$ is a vector that denotes all LECs. In this work we use nonlocal regulators with a cutoff $\Lambda = 394$ MeV/c.

Recently, model reduction methods [41] such as eigenvector continuation (EC) [42,43], has proven to be both efficient and accurate for emulating the output of *ab initio* computations of both scattering [44,45] and bound-state observables [25–28,46]. These methods employ the fact that the eigenvector trajectory generated by smooth changes of the Hamiltonian matrix is well approximated by a very low-dimensional manifold [42]. Following Refs. [25,26] we can therefore obtain good approximations of the ground-state of a target Hamiltonian $H(\vec{\alpha}_\odot)$ by projecting it on a subspace of $N_{\rm sub}$ different ground-state training eigenvectors and solving the corresponding $(N_{\rm sub} \times N_{\rm sub})$-dimensional generalized eigenvalue problem. In this work we employ emulators for ^{2,3}H and ^{4}He for history matching, and the SPCC method with single, double, and leading-order triple excitations (CCSDT-3) for subsequent model calibration on ^{16}O (see Ref. [7] for details). We also construct a new emulator for ^{6}Li based on Ref. [28] for model checking. Here we used $N_{\rm sub} = 32$ training points reaching a relative accuracy of 10^{-3} for the nonimplausible parametrizations [47].

In this Letter we use the coupled-cluster method [38,48–59] within the doubles approximation (CCD) and solve for pure neutron and symmetric nuclear matter on a cubic lattice in momentum space using periodic boundary conditions [30]. The model-space has $(2n_{\rm max}+1)^3$ momentum points with $n_{\rm max} = 4$. We use 132 nucleons for SNM and 66 neutrons for PNM which allows us to minimize finite-size effects [30,60]. We then use the EC-inspired SPCC method [25] to construct subspace emulators at five different nuclear densities. Since the subspace projected coupled-cluster Hamiltonian is non-Hermitian, the variational theorem does not hold [61]. This might lead to the appearance of "spurious" states in the subspace spectrum that are lower in energy than the corresponding full-space coupled-cluster solution for certain combinations of the LECs. These states appear due to the nonsymmetric treatment of the left and right biorthogonal coupled-cluster states [56]. Therefore, we have developed a new algorithm—called small-batch voting—which allows us to identify the physical ground state using a set of different subspace projections. This algorithm employs the strong sensitivity of spurious states on the specific choice of basis, and the contrasting stability of physical states. Details of this algorithm are given in the companion paper [37].

Results. We used history matching to collect a large number of 1.7×10^6 model parametrizations that exhibit acceptable (or at least nonimplausible) fits to the history-matching observables. The latter include a total of 36 neutron-proton phase shifts in S and P waves up to $T_{\rm lab} = 200$ MeV scattering energy and six bound-state observables for $A = 2, 3, 4$ systems. This set is relevant for model calibration, allows fast model simulation or emulation, and permits the construction of simple implausibility measures. In the final wave we defined the nonimplausible volume using a rotated hyperrectangle that captured parameter correlations and allowed to significantly increase the number of collected nonimplausible samples. Further details of the history match are presented in the companion paper [37]. We then strategically selected 64 of the most accurate nonimplausible samples for which we performed full CCD computations for SNM and PNM at five different densities $\rho \in \{0.12, 0.14, 0.16, 0.18, 0.20\}$ fm^{-3}. Together with small-batch voting this allowed us to create SPCC emulators for E/A and E/N at these densities. Finally, the nuclear matter EOS around saturation could be obtained by interpolation using Gaussian processes [62] as described in more detail in Ref. [37].

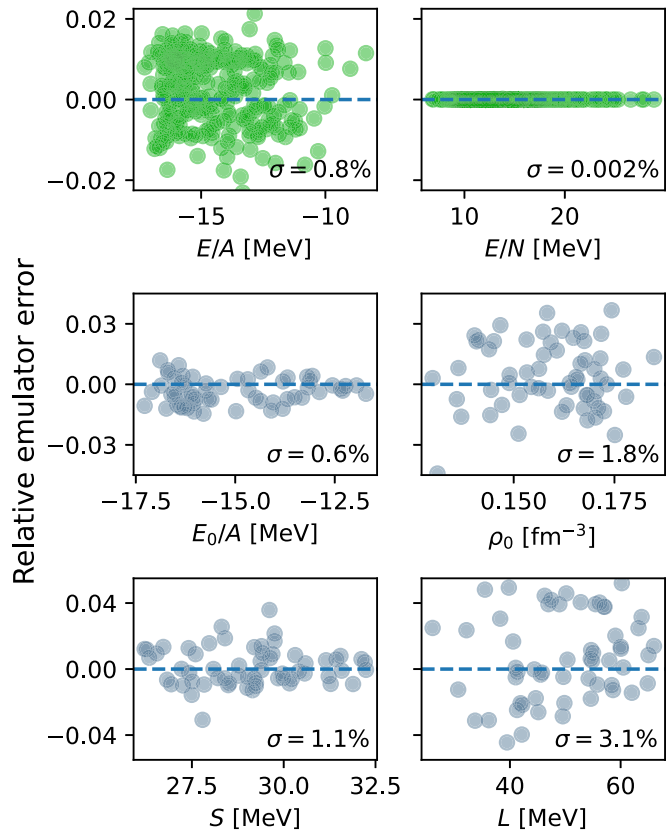

FIG. 1. Cross-validation of the SPCC emulator with exact CCD calculations using 50 interaction samples. Shown here from top to bottom is the nuclear matter saturation density (ρ_0), saturation energy (E_0/A), and symmetry energy (S). Histograms of relative errors are shown in the right column.

Cross validation of emulator performance is shown in Fig. 1. The 50 validation interactions were randomly selected from the nonimplausible volume in a space-filling manner. We conclude that our emulators predict the energy per particle for SNM (PNM) with $<10^{-2}$ ($<10^{-4}$) relative precision at a computational cost that is six (eight) orders of magnitude smaller

than the full solution. Furthermore, Gaussian-process interpolation of the emulated EOS allows us to extract empirical nuclear-matter properties with ≈1% precision (increasing to 3% and 10% for derivative quantities L and K, respectively).

Having access to fast and accurate emulators, and having identified a nonimplausible region in the parameter space of our chiral interaction model, we can proceed to study the general behavior of nuclear matter model predictions and possible correlations between different properties of these systems. Here we are not interested in the usual optimization approach that results in a single ("best fit") model parametrization. Instead, we consider all nonimplausible samples from the history match. About 73% of these samples predict saturation within the studied density region and are kept for further consideration. The outputs from the nuclear matter emulators for these 1.2×10^6 interaction samples are shown in the upper triangle of Fig. 2. Here we have applied a density-dependent energy shift to approximately account for triples corrections [37].

We observe a strong anticorrelation between the saturation energy E_0/A and the saturation density ρ_0 (Pearson correlation coefficient $r = -0.92$). This finding is in agreement with the Coester line [63] for nucleon-nucleon interactions. Similarly, the symmetry energy S and its slope L show a positive correlation ($r = 0.60$). These correlations have been seen in DFT calculations [64,65] and have been indicated with small families of EFT-inspired [15] or (Δ-less) chiral interactions [16]. The comparison with empirical nuclear matter properties reveals that the model predictions from the history match are clustered in a region with too small $|E_0/A|$, ρ_0, and S. This finding is consistent with previous results from various few-body optimized interactions [20,36,66].

The nonimplausible predictions of nuclear matter properties that is shown in the upper triangle of Fig. 2 is a form of Bayes linear forecasting. By just considering expectation values such as means and variances—thereby avoiding the full probabilistic specification of uncertain quantities—we made the analysis simpler and more technically straightforward. While this allowed us to identify the parameter region of interest and to explore the model's forecasting capabilities, we now make an effort to extract a posterior predictive distribution (PPD) with which we can make probabilistic statements.

First, we revisit all remaining interaction parametrizations and keep only those that survive an extra implausibility analysis involving the selected S and P wave phase shifts and that give an unbound $^1S_0$ ground-state in the neutron-proton system. This step results in a significant reduction to 8218 acceptable samples. Second, we introduce a set of calibration observables $\mathcal{D}_{\rm cal}$ and a normally distributed likelihood, $\mathcal{L}(\mathcal{D}_{\rm cal} \,|\, \vec{\alpha})$, assuming independent experimental, method, emulator, and model errors [37]. At this stage we employ the established method of sampling and importance resampling [39,40] to approximately extract samples from the parameter posterior $\mathrm{pr}(\vec{\alpha} \,|\, \mathcal{D}_{\rm cal}, I)$. In this step we assume a uniform prior probability for all nonimplausible samples [71].

In this work we especially considered two different sets of model calibration data: (i) $\mathcal{D}_{\rm cal} = \mathcal{D}_{A=2,3,4}$ encompassing binding energies and point-proton radii of ^{2,3}H and ^{4}He plus the quadrupole moment of the deuteron, and (ii) $\mathcal{D}_{\rm cal} = \mathcal{D}_{A=2,3,4,16}$ where we complemented the above set of observables with the energy and radius of ^{16}O. Note that our choice of history-matching observables allows for both PPD resampling analyses to be performed from the same set of nonimplausible prior samples.

Having access to approximate parameter posteriors we first extract samples from the model PPD defined as $\mathrm{PPD_{th}} = \{\mathbf{y}_{\rm th}(\vec{\alpha}) : \vec{\alpha} \sim \mathrm{pr}(\vec{\alpha} \,|\, \mathcal{D}_{\rm cal}, I)\}$. As a nontrivial model validation we predict the ^{6}Li threshold energy $S_d = E(^2\mathrm{H}) + E(^4\mathrm{He}) - E(^6\mathrm{Li})$ using our EC emulators. The 90% credible intervals are $[-0.14, 1.54]$ MeV and $[1.23, 1.84]$ MeV for $\mathrm{PPD_{th}}$ with $\mathcal{D}_{A=2,3,4}$ and $\mathcal{D}_{A=2,3,4,16}$ calibration data, respectively. Both predictions are consistent with the experimental value $S_d = 1.474$ MeV [72], but the latter one is significantly more precise.

We then predict nuclear matter properties. For these predictions we collect samples from the full PPD, which includes the EFT truncation error, CC method errors, and the SPCC emulator error (estimated from cross validation shown in Fig. 1). The density dependence and relevant cross correlation of these errors are described by a Bayesian machine-learning error model [19,20,37]. Our strategic emulator construction—using training samples with high importance weight—implies that up to 60% of resampled interactions have zero emulator error. Using the two different sets of calibration data, $\mathcal{D}_{A=2,3,4}$ and $\mathcal{D}_{A=2,3,4,16}$, we compare the resulting PPDs that we label $\mathrm{PPD}_{A=2,3,4}$ and $\mathrm{PPD}_{A=2,3,4,16}$, respectively. These are shown in the lower triangle of Fig. 2.

The marginal distributions on the diagonal reveal that ρ_0, E_0/A, and S for $\mathrm{PPD}_{A=2,3,4}$ are characterized by low precision and mild tension with the empirical region—as previously observed with the non-importance-weighted samples. In other words, even by enforcing a higher accuracy for two- and few-body systems via the data likelihood, the general description of nuclear matter properties is not improved. On the other hand, the predictions become more precise and accurate when we include the ^{16}O observables. In particular, the saturation point is more precisely predicted while its mode shifts to larger saturation density and binding energy. We actually find that $\mathrm{PPD}_{A=2,3,4}$ displays a significant asymmetry in some dimensions, e.g., ρ_0, which hints to a possible bimodality. Samples from the tail region of $\mathrm{PPD}_{A=2,3,4}$ correspond largely to the mode of $\mathrm{PPD}_{A=2,3,4,16}$. This finding shows that the emergence of saturation, represented by the position and shape of this mode, depends on the choice of calibration observables.

Our predictions of the nuclear EOS around saturation, with quantification of relevant sources of uncertainty, can serve as an important anchor for extrapolations to higher densities and studies of neutron-star physics. To illustrate, we show a simple extrapolation based on $\mathrm{PPD}_{A=2,3,4,16}$—which gives the most precise predictions—for empirical parameters in Fig. 3. It highlights the fact that an uncertainty band is obtained, which is key for rigorous error estimates at higher densities. A multivariate Gaussian approximation of our PPD for nuclear-matter parameters is provided as Supplemental Material [67]. The interaction samples with importance weights are provided in the companion paper [37].

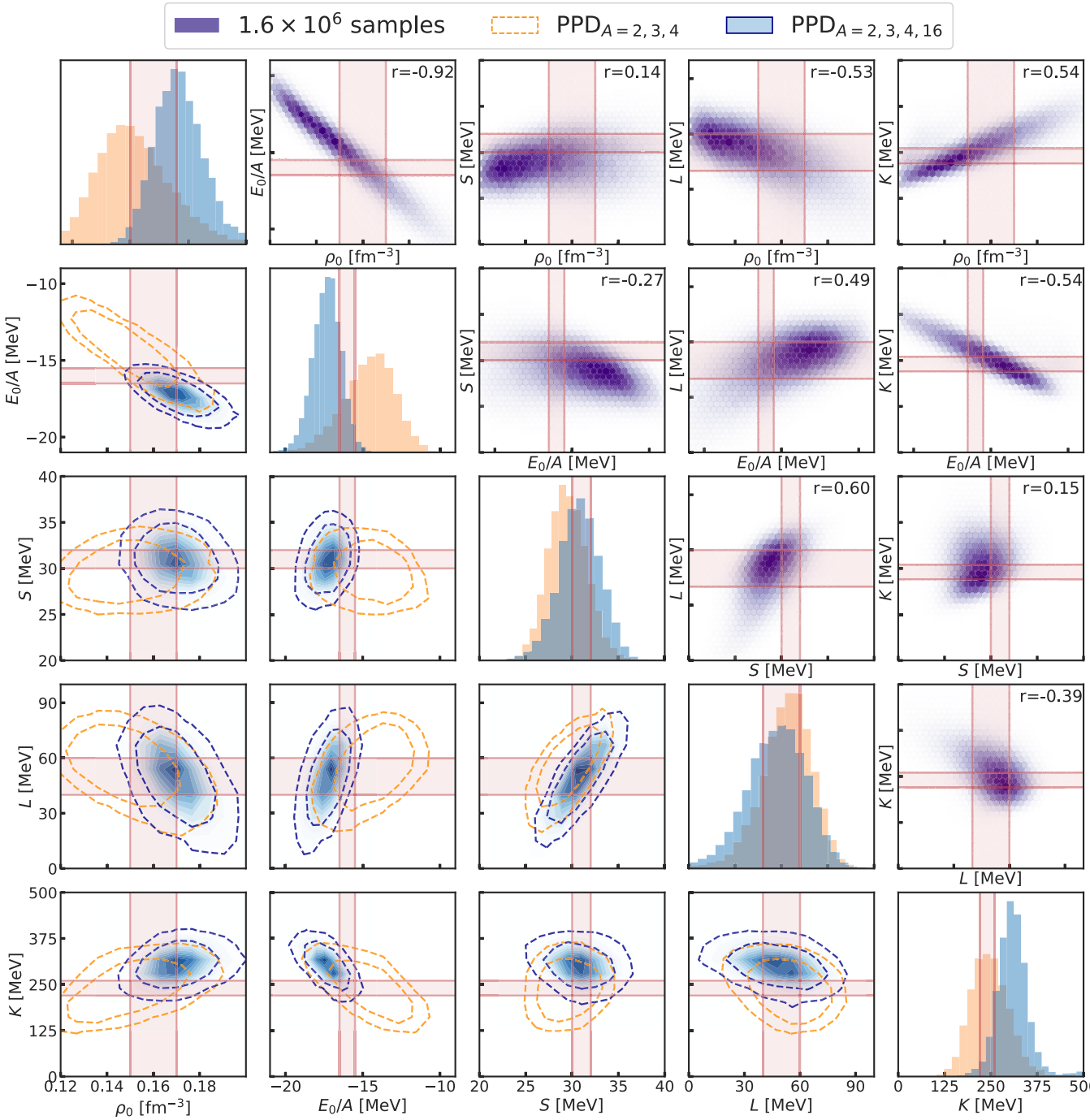

FIG. 2. Upper triangle: nuclear matter emulator output (saturation density ρ_0, saturation energy E_0/A, symmetry energy S, symmetry energy slope L and incompressibility K) for the nonimplausible interactions from the fifth wave of history matching. The axes limits are the same as in the corresponding panels in the lower triangle. Lower triangle and diagonal: PPDs for nuclear matter properties using two different PDFs for the LECs plus error sampling. These predictions are based either on few-body ($A = 2, 3, 4$) calibration data (orange PPD) or the addition of ^{16}O to the calibration dataset (blue PPD). See the Supplemental Material [67] for a Gaussian approximation of $\text{PPD}_{A=2,3,4,16}$. The contour lines on the bivariate distributions denote 68% and 90% credible regions. The red bands indicate empirical ranges for $E_0/A = -16.0 \pm 0.5$ MeV, $\rho_0 = 0.16 \pm 0.01$ fm^{-3}, $S = 31 \pm 1$, $L = 50 \pm 10$, and $K = 240 \pm 20$ MeV from Refs. [68–70].

Summary and outlook. In this work we constructed emulators that accurately reproduce full-space coupled-cluster computations of nucleonic matter starting from Δ-full χEFT at NNLO while reducing the computational cost by several orders of magnitude. The small-batch voting algorithm was developed to remove spurious states that occurred in the SPCC method. Using these tools, together with emulators of light nuclei, we employed history matching to identify more than one million acceptable interaction samples, and could reveal correlations between different properties of

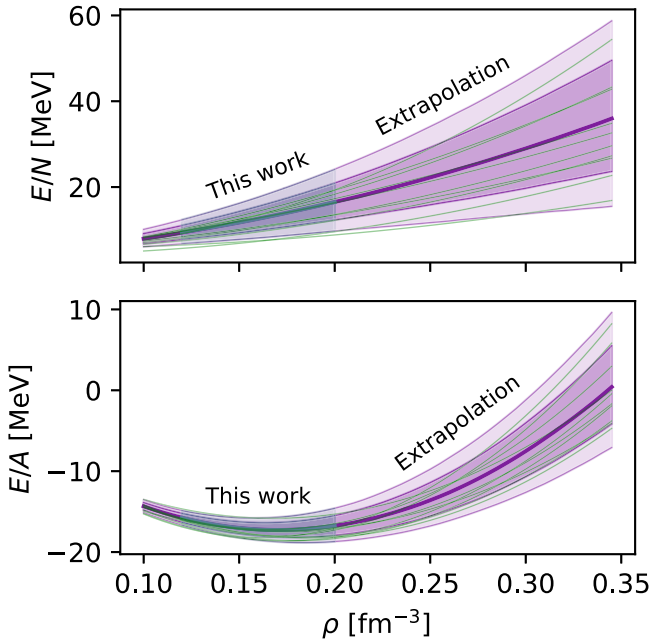

FIG. 3. Dark (light) blue bands show the $\mathrm{PPD}_{A=2,3,4,16}$ for the energy per particle of PNM (upper panel) and SNM (lower panel) computed in the $\rho \in [0.12, 0.20]$ fm^{-3} range. The corresponding purple bands represent simple extrapolations based on the empirical nuclear-matter parameters. For each sample of the PPD the EOS is generated by using the expansion of Ref. [73] and retaining up to quadratic terms in $x = (\rho - \rho_0)/3\rho_0$. Ten such samples are shown with thin, gray lines. The extrapolation uncertainty is not incorporated in the error bands.

infinite nuclear matter. We then employed importance resampling to obtain PPDs and studied the sensitivity to the choice of calibration data. Broad, asymmetric marginal distributions for the saturation energy and density were observed when making predictions conditional on few-nucleon data only, while the predictions become more precise and accurate when adding the ^{16}O energy and radius to the calibration dataset. Binding energies and radii of finite nuclei are obviously useful for model calibration, but are not the only choice. Other observables such as the ^{3}H beta-decay rate and three-nucleon scattering cross sections should also be considered within a statistical framework involving many-body predictions. Ongoing work shows that also these observables can be efficiently computed [74,75] or emulated [27,45]. Our rigorous error bands for the nuclear matter EOS around saturation will be important for advances in studies of dense, neutron-rich matter and for the interpretation of nascent observations from multimessenger astronomy [10–12].

The introduction of small-batch voting demonstrates how emulators can be successfully constructed for challenging many-body observables. Further developments within various many-body computational frameworks are expected to follow [76] in both nuclear physics and beyond. Future work using history matching, Bayesian PPD sampling, and many-body emulators, as exemplified by this study, will help to elucidate the information content of various low-energy observables, the order-by-order convergence of χEFT, and the predictive power of *ab initio* modeling across the nuclear landscape.

Acknowledgments. We thank Andreas Ekström and Thomas Papenbrock for useful discussions. This work was supported by the Swedish Research Council (Grants No. 2017-04234 and No. 2021-04507), the European Research Council under the European Unions Horizon 2020 research and innovation program (Grant No. 758027), and the U.S. Department of Energy under Contract No. DE-AC05-00OR22725 with UT-Battelle, LLC (Oak Ridge National Laboratory). The computations and data handling were enabled by resources provided by the Swedish National Infrastructure for Computing (SNIC) at Chalmers Centre for Computational Science and Engineering (C3SE), and the National Supercomputer Centre (NSC) partially funded by the Swedish Research Council through Grant No. 2018-05973.

[1] R. Machleidt and D. R. Entem, Chiral effective field theory and nuclear forces, Phys. Rep. **503**, 1 (2011).
[2] K. Hebeler, S. K. Bogner, R. J. Furnstahl, A. Nogga, and A. Schwenk, Improved nuclear matter calculations from chiral low-momentum interactions, Phys. Rev. C **83**, 031301(R) (2011).
[3] A. Ekström, G. Baardsen, C. Forssén, G. Hagen, M. Hjorth-Jensen, G. R. Jansen, R. Machleidt, W. Nazarewicz, T. Papenbrock, J. Sarich, and S. M. Wild, Optimized chiral nucleon-nucleon interaction at next-to-next-to-leading order, Phys. Rev. Lett. **110**, 192502 (2013).
[4] A. Ekström, G. R. Jansen, K. A. Wendt, G. Hagen, T. Papenbrock, B. D. Carlsson, C. Forssén, M. Hjorth-Jensen, P. Navrátil, and W. Nazarewicz, Accurate nuclear radii and binding energies from a chiral interaction, Phys. Rev. C **91**, 051301(R) (2015).
[5] W. G. Jiang, A. Ekström, C. Forssén, G. Hagen, G. R. Jansen, and T. Papenbrock, Accurate bulk properties of nuclei from $A = 2$ to ∞ from potentials with Δ isobars, Phys. Rev. C **102**, 054301 (2020).
[6] V. Somà, P. Navrátil, F. Raimondi, C. Barbieri, and T. Duguet, Novel chiral Hamiltonian and observables in light and medium-mass nuclei, Phys. Rev. C **101**, 014318 (2020).
[7] B. S. Hu, W. G. Jiang, T. Miyagi, Z. H. Sun, A. Ekström, C. Forssén, G. Hagen, J. D. Holt, T. Papenbrock, S. R. Stroberg, and I. Vernon, Ab initio predictions link the neutron skin of ^{208}Pb to nuclear forces, Nat. Phys. **18**, 1196 (2022).
[8] P. Maris *et al.* (LENPIC Collaboration), Nuclear properties with semilocal momentum-space regularized chiral interactions beyond N^{2}LO, Phys. Rev. C **106**, 064002 (2022).
[9] S. Elhatisari, L. Bovermann, E. Epelbaum, D. Frame, F. Hildenbrand, H. Krebs, T. A. Lähde, D. Lee, N. Li, B.-N. Lu, M. Kim, Y. Kim, Y. Ma, U.-G. Meißner, G. Rupak, S. Shen, Y.-H. Song, and G. Stellin, Wavefunction matching for solving quantum many-body problems, Nature **630**, 59 (2024).

[10] T. Dietrich, M. W. Coughlin, P. T. H. Pang, M. Bulla, J. Heinzel, L. Issa, I. Tews, and S. Antier, Multimessenger constraints on the neutron-star equation of state and the Hubble constant, Science **370**, 1450 (2020).
[11] S. Huth *et al.*, Constraining neutron-star matter with microscopic and macroscopic collisions, Nature (London) **606**, 276 (2022).
[12] J. M. Lattimer, Constraints on nuclear symmetry energy parameters, Particles **6**, 30 (2023).
[13] E. Khan, J. Margueron, and I. Vidaña, Constraining the nuclear equation of state at subsaturation densities, Phys. Rev. Lett. **109**, 092501 (2012).
[14] G. Hagen, A. Ekström, C. Forssén, G. R. Jansen, W. Nazarewicz, T. Papenbrock, K. A. Wendt, S. Bacca, N. Barnea, B. Carlsson, C. Drischler, K. Hebeler, M. Hjorth-Jensen, M. Miorelli, G. Orlandini, A. Schwenk, and J. Simonis, Neutron and weak-charge distributions of the ^{48}Ca nucleus, Nat. Phys. **12**, 186 (2016).
[15] A. Kievsky, M. Viviani, D. Logoteta, I. Bombaci, and L. Girlanda, Correlations imposed by the unitary limit between few-nucleon systems, nuclear matter and neutron stars, Phys. Rev. Lett. **121**, 072701 (2018).
[16] C. Drischler, K. Hebeler, and A. Schwenk, Chiral interactions up to next-to-next-to-next-to-leading order and nuclear saturation, Phys. Rev. Lett. **122**, 042501 (2019).
[17] P. G. Reinhard and W. Nazarewicz, Nuclear charge and neutron radii and nuclear matter: Trend analysis in Skyrme density-functional-theory approach, Phys. Rev. C **93**, 051303(R) (2016).
[18] Z. Carson, A. W. Steiner, and K. Yagi, Constraining nuclear matter parameters with GW170817, Phys. Rev. D **99**, 043010 (2019).
[19] C. Drischler, R. J. Furnstahl, J. A. Melendez, and D. R. Phillips, How well do we know the neutron-matter equation of state at the densities inside neutron stars? A Bayesian approach with correlated uncertainties, Phys. Rev. Lett. **125**, 202702 (2020).
[20] C. Drischler, J. A. Melendez, R. J. Furnstahl, and D. R. Phillips, Quantifying uncertainties and correlations in the nuclear-matter equation of state, Phys. Rev. C **102**, 054315 (2020).
[21] U. von Toussaint, Bayesian inference in physics, Rev. Mod. Phys. **83**, 943 (2011).
[22] I. Vernon, M. Goldstein, and R. G. Bower, Galaxy formation: A Bayesian uncertainty analysis, Bayesian Anal. **5**, 619 (2010).
[23] I. Vernon, M. Goldstein, and R. Bower, Galaxy formation: Bayesian history matching for the observable universe, Stat. Sci. **29**, 81 (2014).
[24] I. Vernon, J. Liu, M. Goldstein, J. Rowe, J. Topping, and K. Lindsey, Bayesian uncertainty analysis for complex systems biology models: Emulation, global parameter searches and evaluation of gene functions, BMC Syst. Biol. **12**, 1 (2018).
[25] A. Ekström and G. Hagen, Global sensitivity analysis of bulk properties of an atomic nucleus, Phys. Rev. Lett. **123**, 252501 (2019).
[26] S. König, A. Ekström, K. Hebeler, D. Lee, and A. Schwenk, Eigenvector continuation as an efficient and accurate emulator for uncertainty quantification, Phys. Lett. B **810**, 135814 (2020).
[27] S. Wesolowski, I. Svensson, A. Ekström, C. Forssén, R. J. Furnstahl, J. A. Melendez, and D. R. Phillips, Rigorous constraints on three-nucleon forces in chiral effective field theory from fast and accurate calculations of few-body observables, Phys. Rev. C **104**, 064001 (2021).
[28] T. Djärv, A. Ekström, C. Forssén, and H. T. Johansson, Bayesian predictions for $A = 6$ nuclei using eigenvector continuation emulators, Phys. Rev. C **105**, 014005 (2022).
[29] G. Baardsen, A. Ekström, G. Hagen, and M. Hjorth-Jensen, Coupled-cluster studies of infinite nuclear matter, Phys. Rev. C **88**, 054312 (2013).
[30] G. Hagen, T. Papenbrock, A. Ekström, K. A. Wendt, G. Baardsen, S. Gandolfi, M. Hjorth-Jensen, and C. J. Horowitz, Coupled-cluster calculations of nucleonic matter, Phys. Rev. C **89**, 014319 (2014).
[31] U. van Kolck, Few-nucleon forces from chiral Lagrangians, Phys. Rev. C **49**, 2932 (1994).
[32] T. R. Hemmert, B. R. Holstein, and J. Kambor, Heavy baryon chiral perturbation theory with light deltas, J. Phys. G **24**, 1831 (1998).
[33] N. Kaiser, S. Gerstendörfer, and W. Weise, Peripheral NN-scattering: Role of delta-excitation, correlated two-pion and vector meson exchange, Nucl. Phys. A **637**, 395 (1998).
[34] H. Krebs, E. Epelbaum, and U. G. Meißner, Nuclear forces with Δ excitations up to next-to-next-to-leading order, part I: Peripheral nucleon-nucleon waves, Eur. Phys. J. A **32**, 127 (2007).
[35] E. Epelbaum, H. Krebs, and U.-G. Meißner, Δ-excitations and the three-nucleon force, Nucl. Phys. A **806**, 65 (2008).
[36] A. Ekström, G. Hagen, T. D. Morris, T. Papenbrock, and P. D. Schwartz, Δ isobars and nuclear saturation, Phys. Rev. C **97**, 024332 (2018).
[37] W. G. Jiang, C. Forssén, T. Djärv, and G. Hagen, companion paper, Emulating *ab initio* computations of infinite nucleonic matter, Phys. Rev. C **109**, 064314 (2024).
[38] I. Shavitt and R. J. Bartlett, *Many-Body Methods in Chemistry and Physics* (Cambridge University Press, Cambridge, 2009).
[39] A. F. M. Smith and A. E. Gelfand, Bayesian statistics without tears: A sampling-resampling perspective, Am. Stat. **46**, 84 (1992).
[40] W. Jiang and C. Forssén, Bayesian probability updates using sampling/importance resampling: Applications in nuclear theory, Front. Phys. **10**, 1058809 (2022).
[41] J. A. Melendez, C. Drischler, R. J. Furnstahl, A. J. Garcia, and X. Zhang, Model reduction methods for nuclear emulators, J. Phys. G **49**, 102001 (2022).
[42] D. Frame, R. He, I. Ipsen, D. Lee, D. Lee, and E. Rrapaj, Eigenvector continuation with subspace learning, Phys. Rev. Lett. **121**, 032501 (2018).
[43] A. Sarkar and D. Lee, Convergence of eigenvector continuation, Phys. Rev. Lett. **126**, 032501 (2021).
[44] J. A. Melendez, C. Drischler, A. J. Garcia, R. J. Furnstahl, and X. Zhang, Fast & accurate emulation of two-body scattering observables without wave functions, Phys. Lett. B **821**, 136608 (2021).
[45] X. Zhang and R. J. Furnstahl, Fast emulation of quantum three-body scattering, Phys. Rev. C **105**, 064004 (2022).
[46] P. Demol, T. Duguet, A. Ekström, M. Frosini, K. Hebeler, S. König, D. Lee, A. Schwenk, V. Somà, and A. Tichai, Improved many-body expansions from eigenvector continuation, Phys. Rev. C **101**, 041302(R) (2020).
[47] T. Djärv, JupiterNCSM: A Pantheon of Nuclear Physics, Ph.D. thesis, Chalmers University of Technology, 2021.

[48] F. Coester, Bound states of a many-particle system, Nucl. Phys. **7**, 421 (1958).
[49] F. Coester and H. Kümmel, Short-range correlations in nuclear wave functions, Nucl. Phys. **17**, 477 (1960).
[50] J. Čížek, On the correlation problem in atomic and molecular systems. Calculation of wavefunction components in Ursell-type expansion using quantum-field theoretical methods, J. Chem. Phys. **45**, 4256 (1966).
[51] H. Kümmel, K. H. Lührmann, and J. G. Zabolitzky, Many-fermion theory in expS- (or coupled cluster) form, Phys. Rep. **36**, 1 (1978).
[52] R. F. Bishop, An overview of coupled cluster theory and its applications in physics, Theor. Chim. Acta **80**, 95 (1991).
[53] C. Zeng, D. J. J. Farnell, and R. F. Bishop, An efficient implementation of high-order coupled-cluster techniques applied to quantum magnets, J. Stat. Phys. **90**, 327 (1998).
[54] B. Mihaila and J. H. Heisenberg, Microscopic calculation of the inclusive electron scattering structure function in ^{16}O, Phys. Rev. Lett. **84**, 1403 (2000).
[55] D. J. Dean and M. Hjorth-Jensen, Coupled-cluster approach to nuclear physics, Phys. Rev. C **69**, 054320 (2004).
[56] R. J. Bartlett and M. Musiał, Coupled-cluster theory in quantum chemistry, Rev. Mod. Phys. **79**, 291 (2007).
[57] G. Hagen, T. Papenbrock, D. J. Dean, and M. Hjorth-Jensen, *Ab initio* coupled-cluster approach to nuclear structure with modern nucleon-nucleon interactions, Phys. Rev. C **82**, 034330 (2010).
[58] S. Binder, P. Piecuch, A. Calci, J. Langhammer, P. Navrátil, and R. Roth, Extension of coupled-cluster theory with a noniterative treatment of connected triply excited clusters to three-body Hamiltonians, Phys. Rev. C **88**, 054319 (2013).
[59] G. Hagen, T. Papenbrock, M. Hjorth-Jensen, and D. J. Dean, Coupled-cluster computations of atomic nuclei, Rep. Prog. Phys. **77**, 096302 (2014).
[60] S. Gandolfi, A. Yu. Illarionov, K. E. Schmidt, F. Pederiva, and S. Fantoni, Quantum Monte Carlo calculation of the equation of state of neutron matter, Phys. Rev. C **79**, 054005 (2009).
[61] G. Teschl, *Mathematical methods in quantum mechanics*, Vol. 157 (American Mathematical Soc., Providence, 2014).
[62] C. E. Rasmussen and C. K. I. Williams, *Gaussian Processes for Machine Learning* (The MIT Press, Cambridge, Massachusetts, 2006).
[63] F. Coester, S. Cohen, B. Day, and C. M. Vincent, Variation in nuclear-matter binding energies with phase-shift-equivalent two-body potentials, Phys. Rev. C **1**, 769 (1970).
[64] C. Ducoin, J. Margueron, C. Providência, and I. Vidana, Core-crust transition in neutron stars: Predictivity of density developments, Phys. Rev. C **83**, 045810 (2011).
[65] B. M. Santos, M. Dutra, O. Lourenço, and A. Delfino, Correlations between the nuclear matter symmetry energy, its slope, and curvature from a nonrelativistic solvable approach and beyond, Phys. Rev. C **90**, 035203 (2014).
[66] L. Coraggio, J. W. Holt, N. Itaco, R. Machleidt, L. E. Marcucci, and F. Sammarruca, Nuclear-matter equation of state with consistent two- and three-body perturbative chiral interactions, Phys. Rev. C **89**, 044321 (2014).
[67] See Supplemental Material at http://link.aps.org/supplemental/10.1103/PhysRevC.109.L061302 for numerical parameters of a Gaussian approximation to the PPD.
[68] J. M. Lattimer and Y. Lim, Constraining the symmetry parameters of the nuclear interaction, Astrophys. J. **771**, 51 (2013).
[69] M. Bender, P.-H. Heenen, and P.-G. Reinhard, Self-consistent mean-field models for nuclear structure, Rev. Mod. Phys. **75**, 121 (2003).
[70] S. Shlomo, V. M. Kolomietz, and G. Colo, Deducing the nuclear-matter incompressibility coefficient from data on isoscalar compression modes, Eur. Phys. J. A **30**, 23 (2006).
[71] The prior for $c_{1,2,3,4}$ is the multivariate Gaussian resulting from a Roy-Steiner analysis of πN scattering data [77].
[72] D. R. Tilley, C. M. Cheves, J. L. Godwin, G. M. Hale, H. M. Hofmann, J. H. Kelley, C. G. Sheu, and H. R. Weller, Energy levels of light nuclei $A = 5, 6, 7$, Nucl. Phys. A **708**, 3 (2002).
[73] J. Piekarewicz and M. Centelles, Incompressibility of neutron-rich matter, Phys. Rev. C **79**, 054311 (2009).
[74] S. B. S. Miller, A. Ekström, and K. Hebeler, Neutron-deuteron scattering cross sections with chiral *NN* interactions using wave-packet continuum discretization, Phys. Rev. C **106**, 024001 (2022).
[75] S. B. S. Miller, A. Ekström, and C. Forssén, Posterior predictive distributions of neutron-deuteron cross sections, Phys. Rev. C **107**, 014002 (2023).
[76] T. Duguet, A. Ekström, R. J. Furnstahl, S. König, and D. Lee, Eigenvector continuation and projection-based emulators, arXiv:2310.19419.
[77] D. Siemens, J. Ruiz de Elvira, E. Epelbaum, M. Hoferichter, H. Krebs, B. Kubis, and U. G. Meißner, Reconciling threshold and subthreshold expansions for pion-nucleon scattering, Phys. Lett. B **770**, 27 (2017).